Encoder Power Supply Using Common-Mode Current with a Zero-Phase Inductor and Y-Capacitors

Takumi Nakagaki[1*], Kodai Nishikawa[2], Hiroki Watanabe[2], Jun-ichi Itoh[1], Takeshi Kiribuchi[3]
1 Department of Science of Technology Innovation, Nagaoka University of Technology, Nagaoka, Japan
2 Department of Electrical, Electronics and Information Engineering, Nagaoka University of Technology, Niigata, Japan
3 OMRON Corporation, Kyoto, Japan
*E-mail : s235004@stn.nagaokaut.ac.jp

***Abstract*— This paper proposes an encoder power supply system that utilizes common-mode current in motor-drive applications. Encoder power is delivered through an auxiliary winding added to a zero-phase inductor between the inverter and the motor, without additional magnetic components. Y-capacitors connected between each motor terminal and the motor frame increase the available power by reducing the common-mode impedance. Experimental results confirm that 3.0 nF Y-capacitors increase the encoder power from 0.10 W to 1.43 W. Although the Y-capacitors increase the conducted emission voltage, connecting their midpoints to the DC link midpoint significantly reduces it while maintaining the power supply capability. The output power further increases to 2.23 W with this configuration.**

Keywords— Power supply, Encoder, Common-mode current, Zero-phase inductor, Y-capacitor

I. INTRODUCTION

In recent years, servo drive systems have been increasingly used in smart factories and factory automation systems [1], [2]. These systems require high-precision control. Motors in servo drive systems are typically equipped with encoders that detect rotational speed and rotor position [3]. Each encoder requires both a power cable and a signal cable between the inverter and the motor. In multi-motor systems, the number and total length of these cables increase significantly, thereby increasing wiring complexity and system cost.

As a power supply method for sensors, energy harvesting based on the Wiegand effect has been proposed [4], [5]. Ref. [4] proposed a method for powering electronic devices using pulse voltage generated by magnetization reversal of magnetic materials. Ref. [5] proposed a method for supplying power to a Hall sensor even under extremely low speed operation. On the other hand, these methods cannot provide sufficient power to drive an encoder that requires approximately 1.0 W.

In contrast, power line communication enables the use of encoders while reducing the number of signal cables [6]. Nevertheless, power line communication does not eliminate the dedicated power cable required for each encoder.

This paper proposes an encoder power supply system that utilizes common-mode current. Common-mode current is generated by fluctuations in the common-mode voltage caused by inverter switching. Electromagnetic interference filters and active common-mode cancellers have been used to mitigate the electromagnetic interference caused by this common-mode current in nearby equipment [7]-[9]. One method for suppressing common-mode current is the insertion of a zero-phase inductor. Inserting a zero-phase inductor at the inverter input or output increases the common-mode impedance, thereby suppressing common-mode current. The proposed system powers the encoder by using the zero-phase inductor conventionally used for common-mode current suppression, thereby eliminating the need for an additional transformer. The overall system volume does not increase because no additional magnetic components are required.

The originality of the proposed system lies in supplying power to the encoder by adding a single auxiliary winding to a zero-phase inductor already used for common-mode current suppression. The proposed approach achieves an encoder power supply without additional magnetic components and without increasing the system volume. Y-capacitors are connected between the motor terminals and the motor frame to increase the common-mode capacitance. This increase raises the common-mode current and enhances the power delivered to the encoder. The Y-capacitor capacitance is an important design parameter that determines the power delivered to the encoder, and its proper design ensures the required power is secured. The system uses the common-mode current generated by inverter switching and does not require complex control. On the other hand, increasing the common-mode current may increase device current and inverter losses. In addition, an increase in conducted emission voltage is also a concern. Therefore, this paper experimentally verifies the proposed system using an induction motor and confirms a power delivery of 1.0 W, which satisfies the encoder power requirement. Furthermore, the switching device current stress and the conducted emission voltage with Y-capacitors connected are also evaluated.

II. ENCODER POWER SUPPLY SYSTEM UTILIZING COMMON-MODE CURRENT

Fig. 1 shows the configuration of the proposed encoder power supply system utilizing common-mode current. Power is supplied to the encoder using a zero-phase inductor inserted on the inverter output side. A zero-phase inductor typically consists of the three-phase power lines wound around a common magnetic core in the same direction and with the same number of turns. As a result, the insertion of a zero-phase

inductor reduces common-mode current because it leaves differential-mode currents essentially unaffected while providing high inductance only to the common-mode component. The proposed system adds an auxiliary winding to the zero-phase inductor. The common-mode current is transferred to the auxiliary winding, and drive power for the encoder is obtained from its output. In this paper, the required encoder drive power is set to 1.0 W.

Furthermore, Y-capacitors are connected between the motor terminals and the motor frame, and their neutral point is formed by tying the free ends together. This Y-connection increases the common-mode capacitance to ground. As a result, the common-mode impedance decreases and the common-mode current increases, thereby increasing the available output power to the encoder. The common-mode voltage v_c is generated by the switching operation of the inverter and is defined as

$$v_c = \frac{v_u + v_v + v_w}{3} \quad \text{.....(1).}$$

where v_u, v_v and v_w are the phase voltages. Taking the midpoint of the DC-link voltage V_{dc} as the reference, v_c becomes a four-level waveform with values of $\pm V_{dc}/2$ and $\pm V_{dc}/6$. The common-mode voltage has the same frequency as the inverter switching frequency f_{sw} [10].

Fig. 2 shows a series LCR resonant circuit as the common-mode equivalent circuit of motor drive systems. The waveform of the common-mode current can be approximated by the current waveform of a series LCR resonant circuit. In the proposed system, the common-mode capacitance C mainly consists of the parasitic capacitance of the motor, whereas the common-mode inductance L is mainly determined by the magnetizing inductance of the zero-phase inductor.

The resonance angular frequency ω_n, the peak common-mode current i_1, and damping coefficient ζ are expressed

$$\omega_n = \frac{1}{\sqrt{LC}} \quad \text{.....(2),}$$

$$i_1 = \sqrt{\frac{C}{L}}E \quad \text{.....(3),}$$

$$\zeta = \frac{R}{2}\sqrt{\frac{C}{L}} \quad \text{.....(4).}$$

where E is the amplitude of the common-mode voltage variation, L is the common-mode inductance, C is the common-mode capacitance, and R is the common-mode resistance.

When a zero-phase inductor is inserted, the inductance L and resistance R in the common-mode equivalent circuit increase, whereas the capacitance C remains almost unchanged. As a result, the common-mode impedance increases, and the common-mode current is suppressed.

In contrast, the total common-mode capacitance C_{all} in the proposed system is expressed

$$C_{all} = C_0 + 3C_y \quad \text{.....(5).}$$

where C_0 is the existing capacitance, including the output capacitance of the switching devices and the parasitic capacitance of the motor, and C_y is the capacitance of each Y-capacitor. When the Y-capacitors are connected, the common-mode capacitance increases, whereas the common-mode

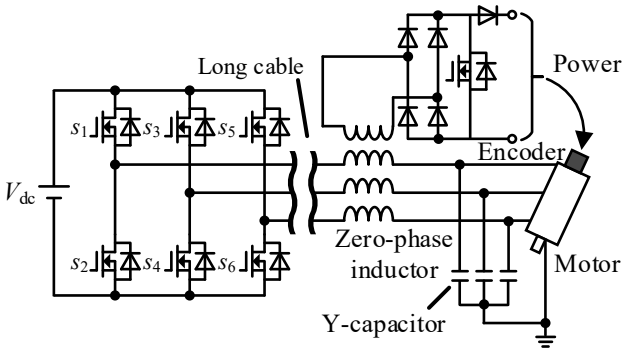

Fig. 1. Circuit configuration of the encoder power supply system that utilizes common-mode current.

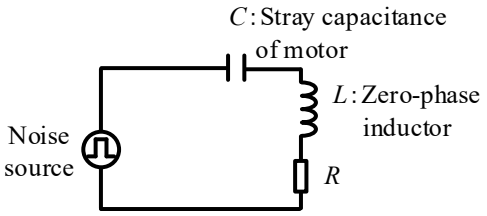

Fig. 2. Common-mode equivalent circuit.

resistance R, common-mode inductance L, and common-mode voltage remain almost unchanged. As a result, the common-mode impedance decreases, and the common-mode current increases. In particular, in the proposed system, the capacitive component dominates the common-mode impedance. According to (3), when the variations in R, L, and the damping effect are sufficiently small, an increase in the total common-mode capacitance leads to an increase in the peak common-mode current.

In the proposed system, this common-mode current is utilized as the encoder power supply through the auxiliary winding of the zero-phase inductor. The output power delivered to the encoder under the present circuit and coupling conditions is approximately expressed as

$$P_o \propto C_{all} \quad \text{.....(6).}$$

Accordingly, the output power delivered to the encoder increases with the Y-capacitor capacitance. The Y-capacitor capacitance is an important design parameter that determines the power delivered to the encoder, and its proper design ensures the required power is secured while minimizing system impact.

III. Experimental Verification of the Proposed System

Fig. 3 shows three experimental circuit configurations used to evaluate the proposed encoder power supply system. Fig. 3(a) shows the configuration without Y-capacitors, which is the basic configuration of the encoder power supply system utilizing common-mode current. However, in this configuration, the output power delivered to the encoder strongly depends on the common-mode impedance, which is determined by factors such as the switching frequency and the parasitic capacitance of the motor. Therefore, it is difficult to supply sufficient power to the encoder.

Fig. 3(b) shows the configuration in which Y-capacitors are connected between each phase terminal and the motor frame. In this configuration, the Y-capacitors are connected in parallel with the common-mode capacitance in Fig. 3(a), thereby increasing the total common-mode capacitance. As a result, sufficient power can be supplied to the encoder without changing the switching frequency or the motor capacitance.

On the other hand, the insertion of the Y-capacitors increases the common-mode current, and its effects must be considered. Specifically, the increase in common-mode current may increase the current flowing through the switching devices, resulting in greater current stress on the devices. In addition, the inverter losses may also increase due to the increase in device current. Furthermore, an increase in the conducted-emission voltage is also a concern.

Fig. 3(c) shows a system configuration that can reduce the conducted-emission voltage when Y-capacitors are connected. Conventionally, the midpoint of the Y-capacitors is connected to the motor frame. In the proposed system, however, this midpoint is connected to the DC-link midpoint instead [11]-[13]. As a result, a common-mode current loop is formed by the three-phase inverter, the zero-phase inductor, and the Y-capacitors. With this configuration, the common-mode noise does not flow out to the LISN side but circulates within the inverter. Since the Y-capacitors are connected near the motor frame, the wiring distance between the midpoint of the Y-capacitors and the DC-link midpoint becomes longer. However, because the proposed system assumes the use of a four-core shielded cable, the wiring complexity does not increase. In all configurations, a line impedance stabilization network (LISN) is connected between the power supply and the inverter in order to define the source impedance and measure the conducted-emission voltage on the power lines. For the basic investigation, the encoder and the front-end diode rectifier are replaced with a resistive load.

Table 1 shows the inverter parameters used in the experiments. The input voltage V_{dc} is set to 330 V, and the switching frequency f_{sw} is 20 kHz. The load resistance is set to 40 Ω, which maximizes the output power when 3.0 nF Y-capacitors are connected. The switching device used is the SCT3030AL, and according to its datasheet, the output capacitance C_{oss} is 180 pF.

Table 2 shows the zero-phase inductor parameters used in the experiments. The zero-phase inductor is configured such that the three-phase power lines are wound once in the same direction, and an auxiliary winding of one turn is wound in the opposite direction to the three-phase lines. A toroidal Finemet core is used. Each winding of the zero-phase inductor is made with a single turn to simplify implementation.

Table 3 shows the parameters of the induction motor. The motor is driven under no-load conditions using sinusoidal PWM with the modulation index set to its maximum, since the common-mode current does not depend on the induction motor load condition. In addition, based on the measured current under rated conditions, the no-load current I_0 is set to 1.95 A.

Fig. 4 shows the common-mode current waveforms without and with Y-capacitors. It is confirmed from Fig. 4 that connecting the Y-capacitors increases the peak value of the common-mode current from 1.24 A to 2.68 A, corresponding to a 2.16-fold increase, and also accelerates its decay. This is because the total common-mode capacitance increases with the Y-capacitors, thereby reducing the common-mode impedance. This result is consistent with the theoretical analysis described above.

Fig. 5 shows the output power characteristics as a function of the Y-capacitor capacitance. The Y-capacitors are connected between each phase and the motor frame. The capacitance is normalized with respect to the output

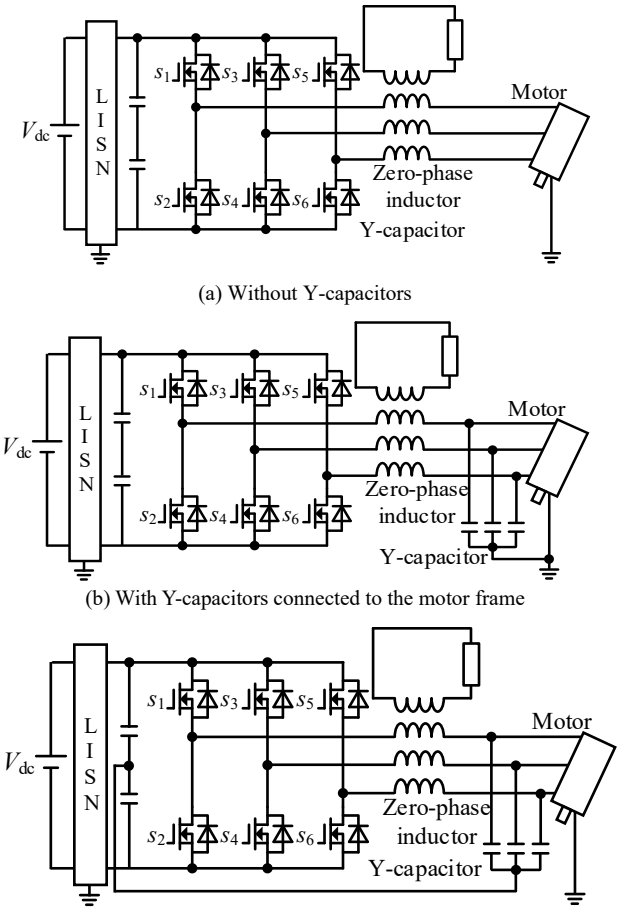

(a) Without Y-capacitors

(b) With Y-capacitors connected to the motor frame

(c) With the midpoint of the Y-capacitors connected to the DC-link midpoint

Fig. 3. Experimental circuit configurations of the proposed encoder power supply system.

TABLE I. OPERATION CONDITIONS OF THREE-PHASE INVERTER.

Parameters	Symbol	Value	
Input voltage of inverter	V_{dc}	330	V
Modulation index(SinPWM)	M	1.0	-
Switching frequency	f_{sw}	20	kHz
Switching device	-	SCT3030AL	
Output capacitance of device	C_{oss}	180	pF
Load resistance	R_L	40	Ω
Inverter output frequency	f	50	Hz

TABLE II. PARAMETERS OF ZERO-PHASE INDUCTOR.

Parameters	Symbol	Value	
AL value@100kHz	AL	15.2	μH/turn^2
Effective cross-section of the core	A_e	213.8	mm^2
Length of the magnetic path	l_e	300.8	mm
Number of turns on the primary-side (Three-phase power line)	N_1	1	turn
Number of turns on the secondary-side (Auxiliary winding)	N_2	1	turn

TABLE III. PARAMETERS OF INDUCTION MOTOR

Parameters	Symbol	Value	
Rated power	P_n	3.7	kW
Rated speed	N_n	1420	r/min
Poles	p	4	–
Rated current	I_n	15	A
Rated voltage	V_n	200	V
No-load current	I_0	1.95	A

capacitance of the switching device. As shown in Fig. 5, the output power increases from 0.102 W without Y-capacitors to 1.43 W with 3.0 nF Y-capacitors, corresponding to an approximately 14.3-fold increase. This increase is attributed to a reduction in the common-mode impedance caused by the additional capacitance, which in turn increases the common-mode current flowing through the encoder-side load resistor. That is, the connection of the Y-capacitors increases the total common-mode capacitance C_{all}, and the resulting increase in the common-mode current leads to an increase in the output power.

The output power increases approximately linearly with the Y-capacitor capacitance. This indicates that the capacitive component dominates the common-mode impedance. This tendency is consistent with the theoretical relationship that the output power is approximately proportional to the total common-mode capacitance. This linear relationship allows estimating the Y-capacitor capacitance required to supply the encoder's power. Accordingly, the Y-capacitor capacitance is an important design parameter that determines the power delivered to the encoder.

On the other hand, excessive Y-capacitance may increase the switching device's drain current and the inverter's losses. Therefore, appropriate capacitance selection is important. Determining the optimal Y-capacitor capacitance remains a subject for future work and should be considered in relation to the motor capacity and the characteristics of the zero-phase inductor.

IV. Effects of Y-Capacitor Connection and Conducted Emission Voltage Reduction Method

A. Evaluation of Device Current and Loss Characteristics

Fig. 6 shows a comparison of the drain-to-source voltage and current waveforms of the U-phase upper-arm switching device under the three configurations. Fig. 6(a) shows the basic configuration without Y-capacitors, Fig. 6(b) shows the configuration with 3.0 nF Y-capacitors connected between each phase terminal and the motor frame, and Fig. 6(c) shows the noise-reduction configuration in which the midpoint of the Y-capacitors is connected to the DC-link midpoint. The waveforms were obtained when the phase of the U-phase voltage command was approximately 40°. As shown in Fig. 6(a), drain current pulsation can be observed during turn-on and turn-off switching operations even without Y-capacitors. When 3.0 nF Y-capacitors are connected as shown in Fig. 6(b), the peak drain currents at turn-on and turn-off are 0.76 A and 0.86 A, respectively, whereas those without Y-capacitors are 0.80 A and 0.46 A. Thus, the turn-on peak current decreases by 5.0%, while the turn-off peak current increases by 86.9%. In addition, the current pulsation becomes longer when the Y-capacitors are connected. These results indicate that increasing the Y-capacitor capacitance increases the current stress on the switching device. When the midpoint of the Y-capacitors is connected to the DC-link midpoint as shown in Fig. 6(c), the peak drain currents at turn-on and turn-off are 0.74 A and 1.0 A, respectively. In addition, current pulsation is observed at turn-off. These results confirm that the proposed conducted-emission voltage reduction method can be applied without significantly increasing the current stress on the switching device.

Fig. 7 shows the peak drain current characteristics as a function of the Y-capacitor capacitance. Fig. 7(a) shows the peak drain current at turn-on, and Fig. 7(b) shows the peak

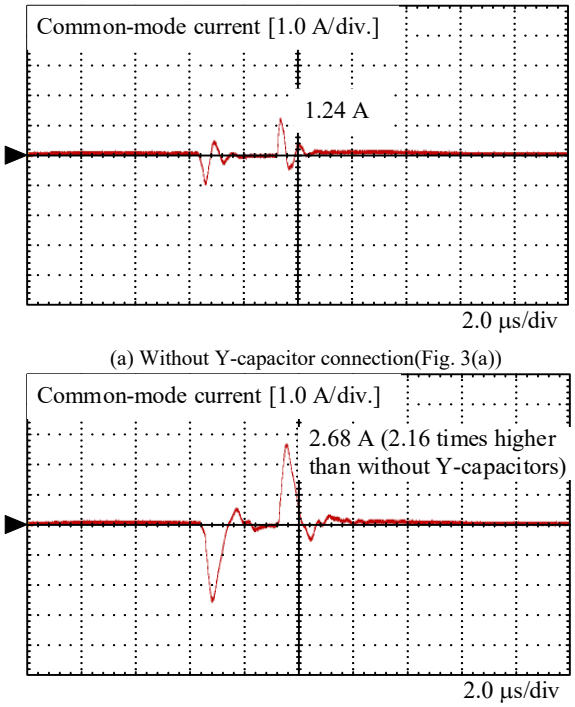

(a) Without Y-capacitor connection(Fig. 3(a))

(b) With Y-capacitor connection (Fig. 3(b))

Fig. 4. Common-mode current waveforms.

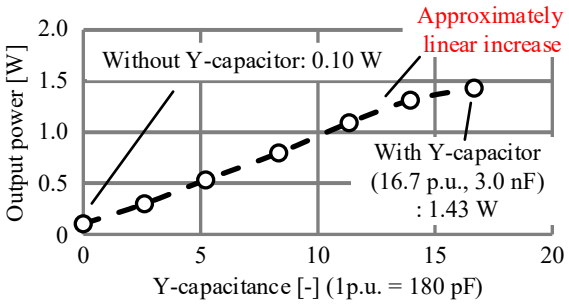

Fig. 5. Output power characteristics as a function of Y-capacitor capacitance.

drain current at turn-off. As shown in Fig. 7(a), the peak drain current at turn-on remains almost unchanged as the Y-capacitor capacitance increases. In contrast, as shown in Fig. 7(b), the peak drain current at turn-off increases with the Y-capacitor capacitance. However, this increase is more gradual than the increase in output power shown in Fig. 5. This behavior is attributed to the suppression of the peak current increase by the leakage inductance of the zero-phase inductor. As a result, when 3.0 nF Y-capacitors, corresponding to 16.7 times the output capacitance of the switching device, are connected, the output power becomes 14.3 times that without the Y-capacitors. In contrast, the peak drain current becomes only 1.87 times that without the Y-capacitors. Therefore, the addition of the Y-capacitors greatly contributes to an increase in output power, while the increase in current stress on the switching device remains relatively limited.

Fig. 8 shows the inverter loss characteristics as a function of the Y-capacitor capacitance. As shown in Fig. 8, the inverter loss remains almost constant at approximately 7.0 W even as the Y-capacitor capacitance increases. This is because the increase in drain current caused by connecting the Y-capacitors is small compared with the no-load current of the induction motor. The slight variation in the inverter loss characteristics is considered to be due to measurement error.

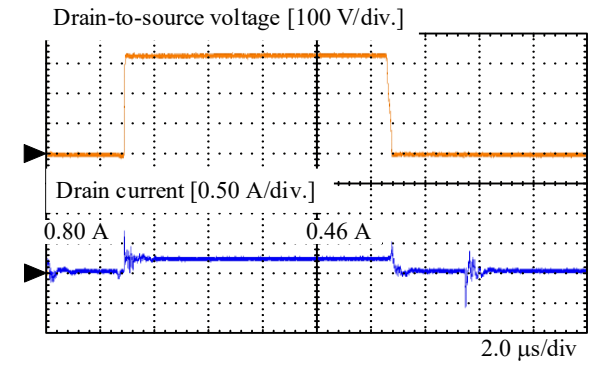

(a) Without Y-capacitor connection(Fig. 3(a))

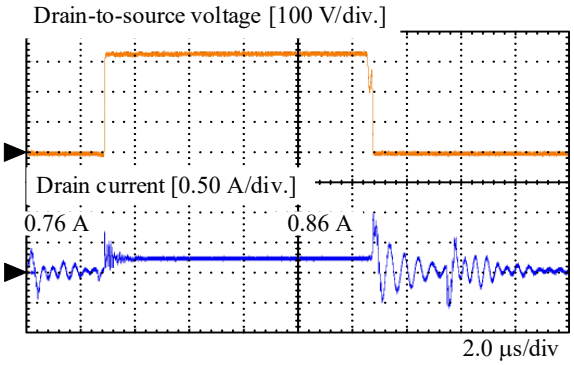

(b) With Y-capacitors connected to the motor frame (Fig. 3(b))

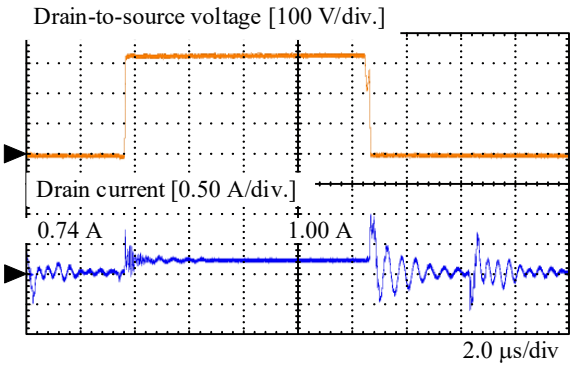

(c) With the midpoint of the Y-capacitors connected to the DC-link midpoint (Fig. 3(c))

Fig. 6. Comparison of drain-to-source voltage and drain current waveforms of the U-phase upper-arm switching device under three configurations.

In addition, the output power of the proposed system was 2.23 W when the midpoint of the Y-capacitors was connected to the DC-link midpoint, which was 1.56 times that obtained when the midpoint of the Y-capacitors was connected to the motor frame. This increase is attributed to a reduction in the common-mode impedance because the common-mode current loop no longer includes the parasitic capacitance of the motor. Therefore, the proposed system provides a sufficient margin over the 1.0 W required to drive the encoder, making it possible to further reduce the required Y-capacitor capacitance.

B. Evaluation of Conducted Emission Voltage

Fig. 9 shows the conducted emission voltage without and with Y-capacitors. The conducted emission voltage was measured using a spectrum analyzer with the output signal from the LISN. The measurement range was set from 150 kHz to 30 MHz, and the RBW was set to 10 kHz. Fig. 9(a) shows

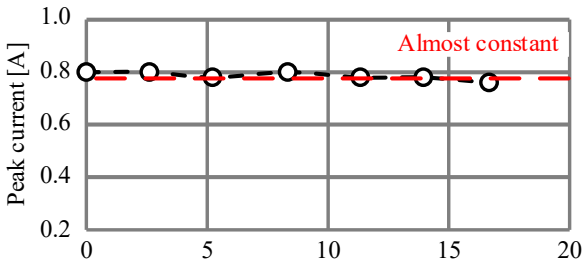

(a) Peak drain current at turn-on

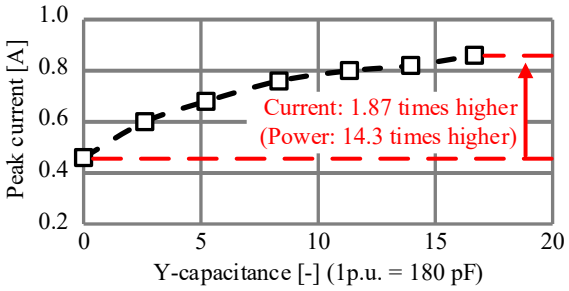

(b) Peak drain current at turn-off

Fig. 7. Peak drain current characteristics as a function of Y-capacitor capacitance.

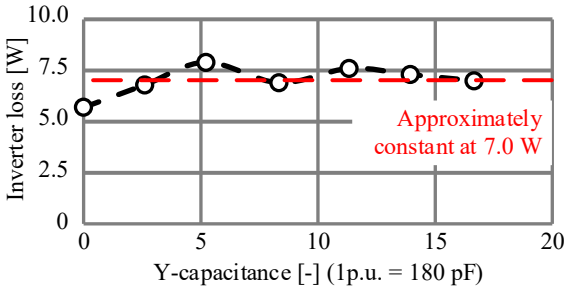

Fig. 8. Inverter loss characteristics versus Y-capacitor capacitance.

the conducted emission voltage without and with 3.0 nF Y-capacitors connected to the motor frame. As shown in Fig. 9(a), connecting the Y-capacitors increases the conducted-emission components in the frequency ranges of 150 kHz to 1 MHz and 2 to 4 MHz. These increases deteriorate the EMI performance of the system, and countermeasures are therefore required. These components are considered to correspond to the current oscillation at turn-off shown in Fig. 6(b).

Fig. 10 shows the conducted emission voltage under the three configurations and their differences. As shown in Fig. 10, connecting the midpoint of the Y-capacitors to the DC-link midpoint significantly reduces the components in the frequency range from 150 kHz to 1 MHz that increase due to the Y-capacitor connection. Compared with the case without Y-capacitors, the noise level is slightly higher. However, it is sufficiently reduced. On the other hand, the component around 2 MHz remains. This component is caused by resonance between the Y-capacitors and the common-mode inductance.

In summary, the Y-capacitors effectively increase the output power of the proposed system with only a limited increase in device current stress and inverter loss. Although the Y-capacitors increase the conducted-emission voltage, connecting their midpoint to the DC-link midpoint significantly reduces the emission while maintaining sufficient encoder power. Therefore, the proposed configuration achieves both improved power supply performance and conducted emission reduction.

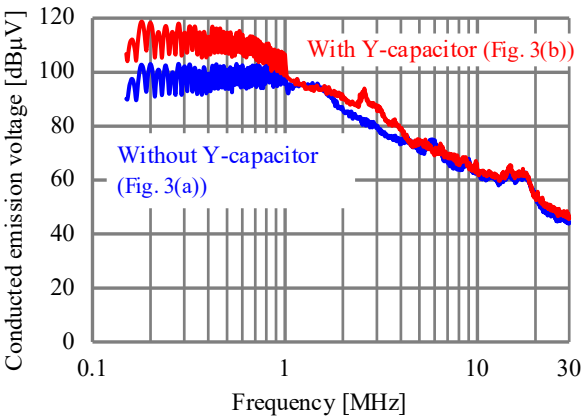

(a) Conducted emission voltage with and without the Y-capacitors

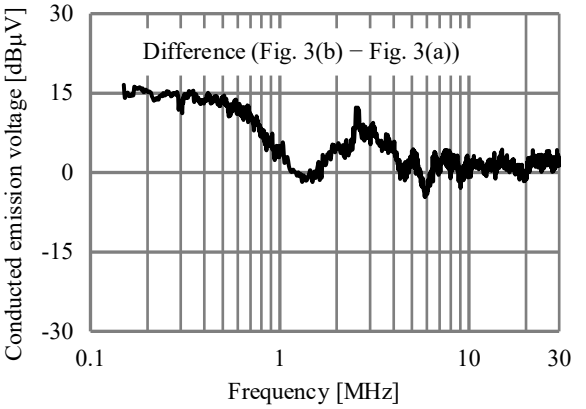

(b) Difference between the conducted emission voltages with and without the Y-capacitors

Fig. 9. Conducted emission voltage of the proposed system.

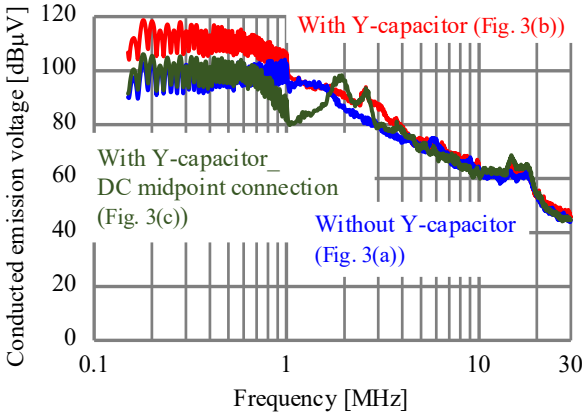

(a) Conducted emission voltage with and without the reduction method and without the Y-capacitors

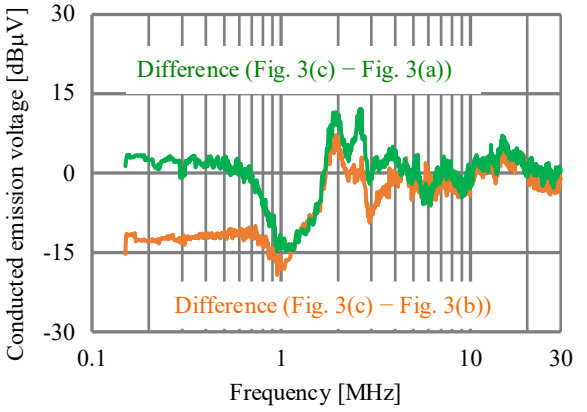

(b) Difference in conducted emission voltage between the cases with and without the reduction method

Fig. 10. Conducted emission voltage of the encoder DC power supply system with the reduction method applied.

V. Conclusion

This paper proposed an encoder power supply system that utilizes common-mode current in motor drive systems. Power transfer is achieved by adding an auxiliary winding to a zero-phase inductor already used for common-mode current suppression. This configuration requires no additional magnetic components and therefore does not increase the system volume.

Y-capacitors were connected between the motor terminals and the motor frame in order to increase the encoder output power. Experimental results showed that connecting 3.0 nF Y-capacitors increased the encoder output power from 0.10 W to 1.43 W. However, the Y-capacitor connection also increased the conducted emission voltage. A configuration in which the midpoint of the Y-capacitors is connected to the midpoint of the DC link was proposed to address this issue. This configuration allows the common-mode noise to circulate within the inverter and significantly reduces the conducted emission voltage.

Experimental results confirmed that the proposed reduction method effectively suppresses the conducted emission voltage while maintaining the encoder power supply performance. In addition, the output power increased to 2.23 W, which was 1.56 times that obtained when the midpoint of the Y-capacitors was connected to the motor frame. The output power exceeded the required 1.0 W for encoder operation. This result indicates that the required Y-capacitor capacitance can be further reduced while maintaining sufficient power for encoder operation. Therefore, the proposed system can provide sufficient power for the encoder without increasing the system volume.

Future work will clarify the design guidelines for the zero-phase inductor and investigate the applicability of the proposed system under a diode rectifier load.

References

[1] R. Kitayoshi, Y. Yoshiura, and Y. Kaku, “Σ-X Series: AC Servo Drive for Achievement of Digital Solution”, IEEJ Journal of Industry Applications, Vol. 12, No. 5, pp. 859-867, 2023.

[2] K. Shimamoto, and T. Murakami, “Wide-Bandwidth Estimation of Cross-Coupling Factors for Position-Sensorless Control”, IEEJ Journal of Industry Applications, Vol. 14, No. 1, pp. 111-119, 2025.

[3] T. Ohhira, Y. Watanabe, and H. Hashimoto, “Improved Angle Calculation Method of MAE-DMFD”, IEEJ Journal of Industry Applications, Vol. 13, No. 6, pp. 625-632, 2024.

[4] Y. Takemura, N. Fujinaga, A. Takeuchi, and T. Yamada, “Batteryless Hall Sensor Operated by Energy Harvesting From a Single Wiegand Pulse”, IEEE Transactions on Magnetics, Vol. 53, No. 11, pp. 1-6, 2017.

[5] Y. Takemura, and A. Matsushita, “Frequency dependence of output voltage generated from bundled compound magnetic wires”, IEEE Transactions on Magnetics, Vol. 37, No. 4, pp. 2862-2864, 2001.

[6] M. V. Ribeiro, M. De L. Filomeno, Â. Camponogara, T. R. Oliveira, T. F. Moreira, S. Galli, and H. V. Poor, “Seamless Connectivity: The Power of Integrating Power Line and Wireless Communications”,

IEEE Communications Surveys & Tutorials, Vol. 26, No. 1, pp. 1034-1045, 2024.

[7] S. Wang, Y. Y. Maillet, F. Wang, D. Boroyevich, and R. Burgos, “Investigation of Hybrid EMI Filters for Common-Mode EMI Suppression in a Motor Drive System”, IEEE Transactions on Power Electronics, Vol. 25, No. 4, pp. 1034-1045, 2010.

[8] A. Okura, M. Yamaguchi, R. Kusui, H. Watanabe, K. Nishikawa, and J. Itoh, “Volume Minimization of Current Type ACC with Rogowski Coil”, IEEE Applied Power Electronics Conference and Exposition, 2024.

[9] S. Takahashi and R. Kanbayashi, “Passive Cancellation of Input and Output Common-Mode Noise in Three-Phase PWM Inverter-Fed Motor Drive Systems”, IEEJ Journal of Industry Applications, Vol. 14, No. 3, pp. 442-449, 2025.

[10] S. Ogasawara and H. Akagi, “Modeling and Damping of High-Frequency Leakage Currents in PWM Inverter-Fed AC Motor Drive Systems”, IEEE Transactions on Industry Applications, Vol. 32, No. 5, pp. 1105-1114, 1996.

[11] S. Funatsu, H. Matsumori, T. Kosaka, N. Matsui, K. Nakamura, M. Takahashi, S. Taguchi and S. Saha, “GaN-Based Modified Integrated On-Board Charger Configuration Using Minimum Additional Active and Passive Components”, IEEE Transactions on Industry Applications, Vol. 62, No. 2, pp. 3094-3108, 2026.

[12] D. Dong, F. Luo, X. Zhang, D. Boroyevich and P. Mattavelli, “Grid-Interface Bidirectional Converter for Residential DC Distribution Systems – Part 2: AC and DC Interface Design With Passive Components Minimization”, IEEE Transactions on Power Electronics, Vol. 28, No. 4, pp. 1667–1679, 2013.

[13] Y. Zhang, G. Yang, X. He, M. Elshaer, W. Perdikakis, H. Li, C. Yao, J. Wang, K. Zou, Z. Xu and C. Chen, “Leakage Current Mitigation of Non-Isolated Integrated Chargers for Electric Vehicles”, 2018 IEEE Energy Conversion Congress and Exposition (ECCE), 2018.